Temporal behavior of x-ray radiation emitted by subpicosecond KrF-laser-heated carbon preplasmas

C. Wülker, W. Theobald, and F. P. Schäfer
Abteilung Laserphysik, Max-Planck-Institut für biophysikalische Chemie, Postfach 28 41, D-37018 Göttingen, Germany

J. S. Bakos
Department of Plasma Physics, Research Institute for Particle and Nuclear Physics, P.O. Box 49, H-1525 Budapest, Hungary
(Received 28 April 1994)

The soft x-ray radiation intensity ($\lambda \in [5$ Å, 45 Å]) emitted by a carbon plasma after the interaction of a short ultrahigh-intensity KrF laser pulse with preplasmas of different scale lengths was investigated. This was done spectrally and temporally resolved by means of a time-resolving spectrograph. A strong increase in the duration of this radiation with larger scale lengths is observed, which is qualitatively explained by a shift of the heat deposition to smaller densities.

PACS number(s): 52.50.Jm, 52.40.Nk, 52.25.Nr

The necessity of intense sources of x-ray radiation for various applications like x-ray holography leads to vigorous research for solutions. In many cases laser-produced plasmas are part of the systems that meet the requirements of the applications. They are serving as x-ray flash lamps for x-ray microscopy [1] and x-ray lithography [2] or as the active medium for x-ray lasers. The use of short pulses from dense laser-produced plasmas has been proposed for time-resolved x-ray scattering studies [3].

The diversity of the applications demands the ability to fit the properties of the plasmas to their needs. The two most important parameters for this are the temperature and the density of the plasma. The temporal behavior and the spatial gradients of these quantities determine the relative importance of the different processes in the plasma, as there are recombination and ionization of ions, radiative and collisional transitions, heat conduction, etc.

Depending on the wavelength and especially the duration of the plasma-producing laser pulse the gradients of the plasma temperature and density vary substantially. In the case of a laser pulse interacting with a solid body the quantity, which is usually used to characterize the spatial extent of the plasma, is the scale length L. It is defined as the inverse of the logarithmic derivative $[(1/n_e)(dn_e/dx)]^{-1}$ of the density distribution and is equal to L in case of an exponential density profile $n_e(x)=n_{e,0}\exp(-x/L)$. This means that it is inversely proportional to the density gradient of the plasma. $n_{e,0}$ is the relevant maximum electron density of the problem concerned.

When a high-intensity subpicosecond laser is used as the pump pulse the scale length of the resulting plasma is very short [4]. The hottest region of the plasma where most of the energy is deposited is at 1 to 10 times the critical density n_c (the laser frequency ω_L equals the plasma frequency ω_P at the electron density n_c). Due to the strong gradient and the high density, rapid cooling of hot electrons and subsequent quenching of the x-ray emission are expected because of rapid electronic heat conduction into the underlying cold material. For longer scale lengths the emission from the hot plasma region should last longer because the cooling rate of the plasma and the recombination rates drop [5].

One way to create a plasma with a longer scale length that a subpicosecond pulse can interact with, is the production of a preplasma. In previous work [5–7] the amplified spontaneous emission (ASE) of the laser system was used for this purpose which restricts the range of available scale lengths.

In the experiments we present here, the preplasma was produced by a long pulse laser of pulse duration 30 ns. The scale length of the preplasma could be varied up to several μm by changing the delay between the long pulse and a high-intensity subpicosecond laser pulse with a duration of 0.7 ps and an intensity of 4×10^{16} W/cm^2. Both lasers were focused on a highly polished carbon target. At the intensity of 4×10^{16} W/cm^2 the carbon atoms and ions of the preplasma are ionized by field ionization only to the heliumlike ground state with a sufficient rate during the laser pulse [8]. In the hot plasma region mainly, excited states of heliumlike and hydrogenlike carbon ions are reached by collisional excitation and ionization processes. In our experiment the radiation of these states was investigated spectrally and temporally resolved which, therefore, serves as a window to the processes in the hot plasma region.

The geometry of the experiment is shown in Fig. 1. Both laser pulses were focused with overlapping foci onto an optically polished carbon cylinder of 5.70 mm diameter. The long pulse beam (LP) had an angle of incidence of 20° to the target normal. Its focus was of rectangular shape with dimensions 200×300 μm^2 to ensure a nearly one-dimensional expansion of the preplasma and the overlapping of the two foci. The angle of incidence of the short pulse (SP) was 45° with a focal spot diameter of 5 μm. It was p polarized (i.e., parallel to the plane of incidence) for all the reported experiments. The size of the

1063-651X/94/50(6)/4920(6)/$06.00

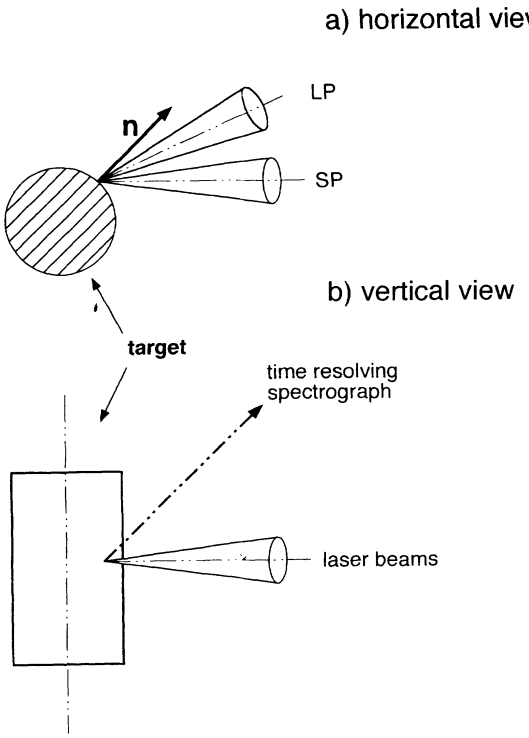

FIG. 1. Geometry of the experiment in (a) horizontal view and (b) vertical view. LP and SP are the long pulse beam and short pulse beam, respectively. The target consists of an optically polished cylinder of glassy carbon (Sigradur).

focal spot was measured by a beam profiler and a microscope before each measuring run. The interaction took place in a vacuum chamber with a background pressure of about 5×10^{-6} mbar.

The SP laser is a hybrid dye–KrF-excimer laser system similar to that described in Ref. [9]. To amplify the second harmonic of the short pulse dye laser radiation in the excimer amplifier, a three-pass off-axis amplification scheme was used [10]. The pulse at the output of this system had an energy of up to 20 mJ and 0.5 ps duration. The effective pulse length on the target was determined by an autocorrelation measurement to be 0.7 ps assuming a Gaussian pulse. The temporal broadening is owing to nonlinear effects and group velocity dispersion in the windows and lenses of the optical path. In the experiments a short pulse energy of 5 mJ on the target was used. The LP laser was a commercial KrF excimer laser (Lambda Physik LPX 100) with a pulse duration of 30 ns. The wavelength of both lasers was 248 nm.

The x-ray photons emitted by the plasma were measured with spectral and temporal resolution by means of a pinhole transmission grating spectrograph connected to a x-ray streak camera. The plasma was observed at an angle of 45° to the plane defined by the two laser beams [see Fig. 1(b)]. The spectrograph consisted of a 100 μm pinhole close to a free standing gold grating with 5000 lines/mm (X-Opt, Gainesville, Florida). This gave a dispersion of 20 Å/mm on the photocathode of the streak camera. The resolution of the pinhole transmission grating spectrograph is determined by the dimensions of the image of the entrance slit on the photocathode of the streak camera. Since no entrance slit was used here (the laser-produced plasma provided the "entrance slit"), the wavelength resolution was limited to 4 Å. The streak camera was a commercial system (Kentech Instruments Ltd, Didcot, England) together with an image intensifier and an optically coupled charge-coupled device (CCD) system. The time resolution of a x-ray streak camera depends on several factors [11]. One of them is the photocathode material which also determines the sensitivity of the system. CsI is well known as the photocathode material with the highest quantum yield but it is not the best for high temporal resolution [12]. In spectrally and temporally resolved measurements the number of photons per channel becomes very small. Therefore we were forced to use the sensitive CsI photocathode which limited the time resolution of the streak camera for the present experimental setup to 6 ps. More details of the time-resolving spectrograph and the usage of different photocathode materials will be given in a subsequent publication [13].

To vary the scale length of the preplasma in the measurements the delay between the two laser pulses was changed. The point where the short pulse laser came right at the leading edge of the long pulse was defined as zero delay. Positive delay meant that the short pulse came later than this leading edge. The jitter of the relative timing was below 5 ns. As an example, a picture from the time-resolving spectrograph (TRS) for the SP alone is shown in Fig. 2. The vertical and the horizontal are the axes of spectral and temporal dispersion, respectively. The figure is a density plot. In the middle of the picture is the zeroth order of the transmission grating with the two first orders extending up and down. It can be clearly seen that the radiation from the helium and hydrogenlike stages of the carbon ions ($\lambda\in[25$ Å, 42Å]) is emitted for a longer time than the radiation at shorter

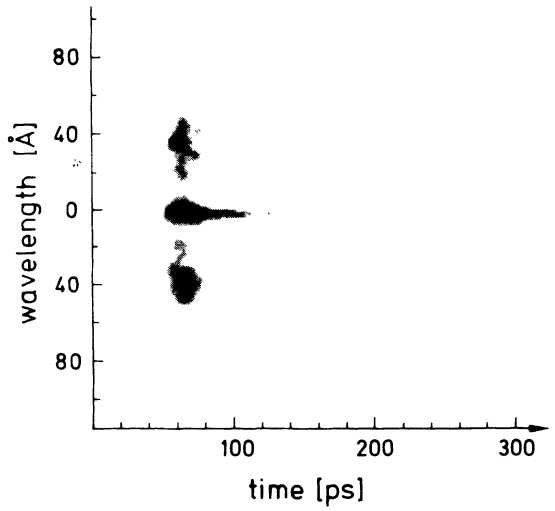

FIG. 2. Density plot from the output of the time-resolving spectrograph. The horizontal axis represents the time, the vertical one the wavelength symmetrically to the zeroth order in the middle of the picture. The picture is a sum of five shots with the SP alone.

wavelengths which comes from bremsstrahlung of hot electrons. The bremsstrahlung is mainly emitted during the presence of the driving laser field. Therefore the temporal width of this radiation reflects the time resolution of the TRS.

The full spectral range of the TRS was determined by the dimensions of the photocathode of the streak camera. For the present setup this was 250 Å for both first orders but the radiation with wavelengths longer than 50 Å was not observed in a significant amount in contrast to an earlier measurement with a time-integrating spectrograph [14]. A reason may be that this radiation was not emitted during the time interval of the temporal window or, which is more probable, the intensity was too small to be detected. Since the main part of this radiation originates from lower density plasma regions [14], its information content about the processes in the dense plasma region is limited.

Figure 3 shows the temporal profiles of radiation for different delays, i.e., for different scale lengths, which were obtained from pictures similar to Fig. 2. The scale lengths for the different profiles range from 0 μm [Fig. 3(a)] up to 316 μm [Fig. 3(e)]. The slices were taken from the zeroth order of the TRS pictures which in principle contains all wavelengths emitted by the laser produced plasma. Due to the restricted sensitivity of the TRS even the zeroth order contained mainly radiation with wavelengths smaller than 50 Å. This was confirmed by a comparison of the slices in Fig. 3 with spectrally integrated profiles of the first orders of the corresponding TRS pictures.

The temporal profiles of the zeroth order are consisting of two parts. These are a short pulse and a then following decay. They were fitted with a combination of a Gaussian with an exponential decay starting at the maximum of the Gaussian. The relative intensities of these two components and the time constant of the exponential decay changed very strongly when a preplasma was present. At minimum amplitude the height of the short pulse was about one third of the one without preplasma. In this case the height of the exponential tail was larger. The temporal integral of the profiles, i.e., the number of collected photons, was slightly higher for the case of 10 and 20 ns delay [Figs. 3(b) and 3(c)]. In case of 40 ns delay there is nearly no difference in the profiles with and without preplasma. This shows that at this delay the 248 nm radiation did not interact with the preplasma any more. Thus the SP produced the hot plasma on the target surface again. Since the pulse duration of the LP was 30 ns, this reflects the hydrodynamic decay of the ex-

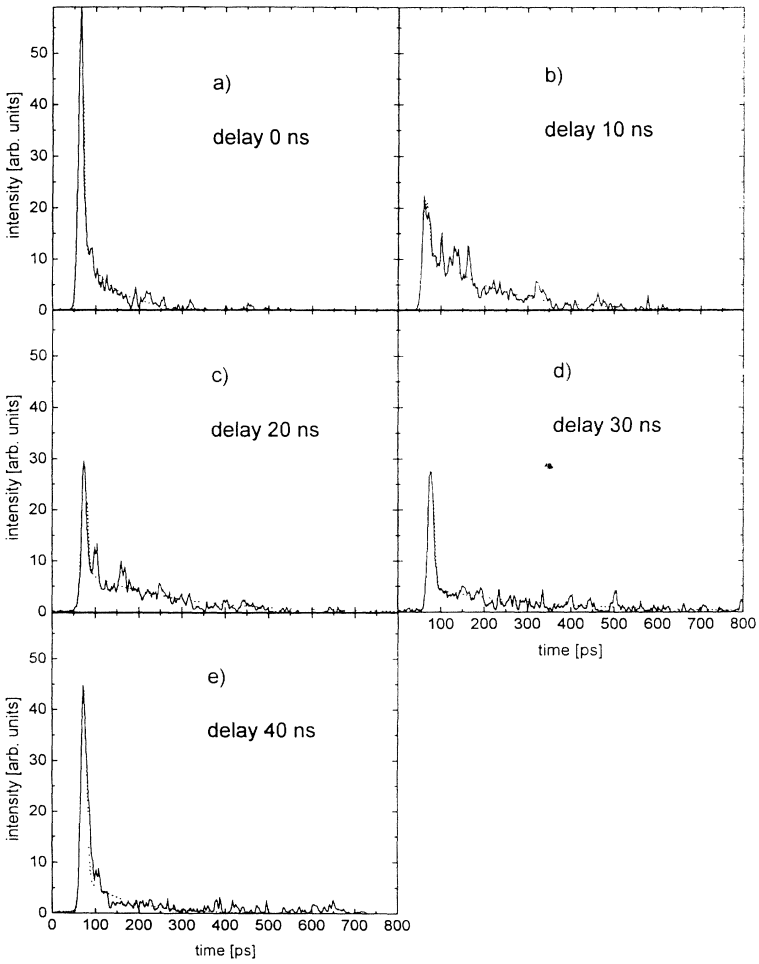

FIG. 3. Temporal profiles of the radiation in the zeroth order with both laser pulses present. All profiles are an average of five shots; the numbers indicate the delay between the pulses. The dotted lines are fits to the profiles (see text).

ponential density profile of the preplasma after the energy transfer from the LP has ceased.

The intensity of the LP was 7×10^8 W/cm^2 for the profiles of Fig. 3. From the change of the temporal behavior at this intensity it must be concluded that the threshold for plasma production with a nanosecond KrF laser is well below this value for carbon. This stresses the necessity of extremely high contrast ratios for investigations of the interaction of ultrahigh intensity lasers with the surface of a solid. We conclude from this measurement that the intensity contrast ratio for the short pulse laser system used in our experiment was at least 10^9.

The change of the decay time of the exponential tails of the plots in Fig. 3 with increasing delay is shown in Fig. 4. Since the scale length is connected with the delay time τ by the relation $L=c_S\tau$, where c_S is the speed of the ions (for our experiment $c_S=8\times10^5$ cm s^{-1} [15]), Fig. 4 shows that the decay time of the radiation is linearly dependent on the scale length. The drop of the decay time at 40 ns shows the "transparency" of the preplasma for the SP as already mentioned.

Figure 5 shows the temporal profiles of the detected radiation for two different wavelengths of Fig. 2, i.e., temporally *and* spectrally resolved profiles for the case of the SP alone. The spectral regions chosen for these slices are $\lambda\in$[26.1 Å, 30.5 Å] and $\lambda\in$[37.7 Å, 42.1 Å]. This means that the first is the record of radiation from the hydrogenlike ions (Ly-β) while the second represents the radiation from the heliumlike ions (He-α). The Lyman-α line of hydrogenlike carbon could not be used for the detection of its presence because the spectral resolution of the TRS did not allow to distinguish between the Ly-α line (33.7 Å) and the He-β line (35.0 Å).

The time duration of the two leading edges of the profiles reflects the time resolution of the TRS of 6 ps. The two curves differ in amplitude, the time of the maximum value and the decay time. The emission of the He-α line culminates 6 ps after the Ly-β and its exponential decay has a decay time of 32±5 ps. The Ly-β line decays faster with a time constant of 15±4.5 ps. When a

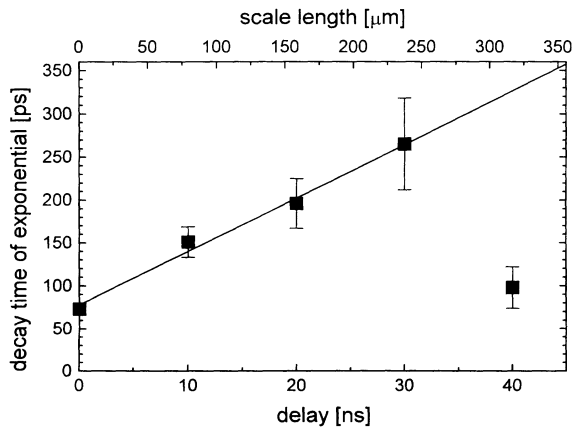

FIG. 4. Decay time of the exponential tail of the profiles in Fig. 3 as a function of the delay. The straight line is a fit to the first four points.

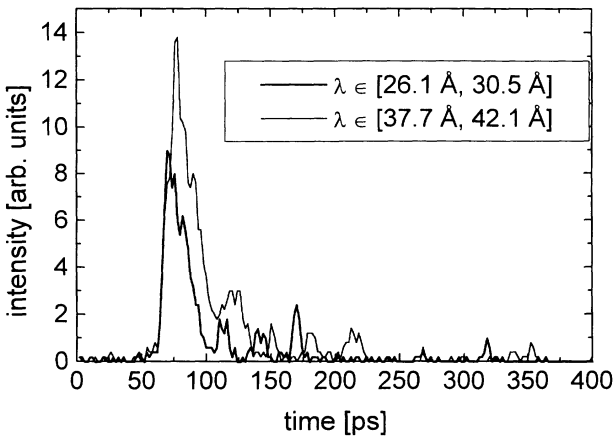

FIG. 5. Temporal profiles of Fig. 2 for the radiation from hydrogenlike carbon (thick line) and heliumlike carbon (thin line).

preplasma was present the curves changed similar to the profiles of Fig. 3.

A quantitative explanation of the lengthening of the radiation decay and especially its linear increase with the scale length needs an extended simulation of all the atomic processes of the ionic species which eventually determine the emission rate of the radiation investigated. These are three body and radiative recombination, ionization, excitation, and deexcitation by electron impact, absorption, and spontaneous emission, as well as, heat conduction and the hydrodynamic evolution of the preplasma. This is out of the scope of the present paper. A qualitative picture may be obtained with some estimates.

As a first approximation we assume a one-dimensional expansion of the preplasma into the vacuum. Thus the preplasma is described by a simple exponential density profile $n(x)=n_0\exp(-x/L)$ with the scale length $L=c_s\tau$ [16]. To distinguish between the effects due to longer scale length or lower densities it is very important to know where in the density profile the laser energy is deposited. For this purpose the density profile was approximated as a stratified medium with constant electron density and refractive index in each layer. The electromagnetic wave equation was solved under this condition by means of a modified version of the computer program of Ref. [4]. This solves the wave equation exactly for each layer and relates the two transverse field components at its boundaries with each other. With appropriate boundary conditions the reflection coefficient and the energy deposition profile for the whole stack can be calculated according to the approach of Ref. [17].

The three parameters governing the absorption are the electron density of the solid material n_0, the collision frequency between the electrons and the ions ν_{ei} (i.e., the damping) and the scale length L. For the calculations n_0 was set to $n_0=30n_c$, where $n_c=2\times10^{22}$ cm^{-3} for our laser wavelength of $\lambda_L=248$ nm. The computer code of Ref. [4] was modified to contain the density dependent collision frequency given in Ref. [18]. The absorption profiles for scale lengths in the range of $0.01\lambda_L$ to $100\lambda_L$ were calculated. An angle of incidence of 45° and p po-

larization were used as in the experiments. The number of layers used for the calculation was 2000 for all scale lengths. This means that their spacing varied from 0.1 Å to 0.1 μm. A test with a higher number of layers yielded no change in the absorption profile.

Figure 6 shows the calculated energy deposition contour plot as a function of the scale length of the exponential density profile and the reduced density n_e/n_c. The corresponding fraction of total absorption is indicated for each contour line. The position of the absorption which is at several times the critical density for the case of the short pulse laser alone ($L/\lambda_L=0.01$) shifts to lower densities with increasing L. The total density width of the absorption is smaller at longer scale lengths, but its full width at half maximum (FWHM) increases. This means that within the approximations of the program the laser energy is deposited at smaller densities for increasing scale length.

The radiation observed is produced by spontaneous emission starting in excited levels of the related ionic stage (stimulated emission is neglected throughout this paper). The duration of its emission depends on the rates of the processes populating and depopulating the upper level of the transition. In general the limiting processes will be either the recombination or the radiative decay, where the corresponding rates have to be taken at the time and the density where the emission occurs. By comparing the observed emission times with the calculated values of these rates it is possible to draw inferences about the physical processes.

When no preplasma was present, the experimental values for the emission times of the Ly-β and the He-α line were 15±4.5 ps and 32±5 ps, respectively. For comparison, shell-averaged values have to be taken [19,20]. This results in radiation decay times of 13.8 ps and 6.0 ps for $C^{5+}(n=3\rightarrow n=1)$ and $C^{4+}(n=2\rightarrow n=1)$.

The value for the Ly-β line agrees well with the experimentally determined one. We conclude from this that for short scale lengths the radiative decay is the process limiting the emission times. Thus the recombination rates must be considerably higher than the radiative decay rates for this case. The experimentally derived value for the He-α line is higher than the calculated one. The reason for this is probably the steady production of C^{4+} by recombination of the C^{5+} ions.

When a preplasma is present, i.e., the scale length is long, we observe a drastic increase of the radiation emission times (see Fig. 3). This cannot be explained by a drop of radiative decay rates. Hence, the recombination becomes the limiting process in the emission from the highly charged ions in the hot plasma region. We thus measure a drop in the recombination rate of at least two orders of magnitude.

For an explanation it is useful to recapitulate the formula for the three-body recombination rate [21]

$$W_r = 4.3\times10^{-32}\ \frac{\mathrm{cm}^6}{\mathrm{s}}\times n_e^2 Z^{-6}\left[\frac{Z^2\mathcal{R}}{T_e}\right]^{9/2}.$$

Z is the charge of the recombining ion, T_e is the electron temperature in eV and the Rydberg constant $\mathcal{R}=13.61$ eV. It is obvious that the recombination rate scales strongly with the electron density and temperature. When we now recall the result of the heat deposition calculation, the situation depicts itself as follows.

(a) For longer scale length plasmas the energy of the short laser pulse is deposited at smaller densities. Through its scaling with the density this has direct consequences on the recombination rates. The recombination becomes slower than the radiative decay of the levels and thus is the limiting factor for the emission times in the experiment.

(b) The heat deposition calculation implies that the half-width of the absorption volume increases for the long scale length preplasmas. Therefore the temperature gradients after the interaction with the short pulse will be smaller. This means that the electronic heat conduction drops, resulting in a longer time with higher electron temperatures. In such a plasma the recombination rates are lower because, for faster electrons, the time spent in the region near to the ion, where recombination is possible, is shorter.

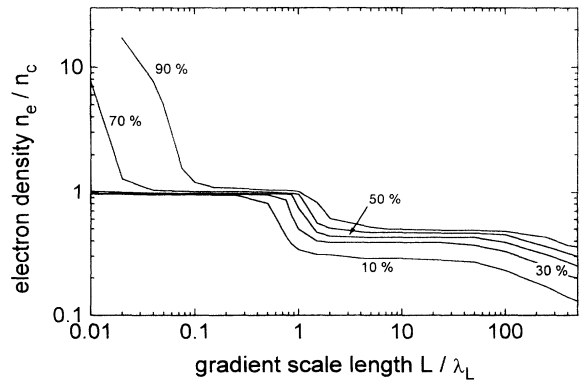

FIG. 6. Lines of constant absorption as a function of the reduced density and the reduced gradient scale length as calculated by solving the Maxwell equations for the experimental parameters. The numbers indicate the fraction of total absorption.

At the present stage we cannot decide, whether one of the above points is dominant or both play a substantial role. This may be accomplished by an extended modeling of the absorption and the atomic processes, e.g., with a self-consistent solution for the Maxwell equation *in combination with* the heat conduction equation.

In conclusion we performed spectrally and temporally resolved measurements of radiation intensity emitted after the interaction of a short ultrahigh-intensity laser with carbon preplasmas of different scale lengths. By the choice of the wavelength region the investigation was concentrated on the dense plasma region. A strong lengthening of the emission time up to a factor of 4 with increasing scale length was observed. This must be explained by the slowing down of the recombination popu-

lating the upper levels of the transitions investigated. A comparison with a calculation of the energy deposition profile indicates that a shift of this profile to lower densities with increasing scale length qualitatively could explain the observed behavior.

We are grateful to R. Fedosejevs for providing us with his computer code for the wave equation solver and B. N. Chichkov for clarifying discussions. It also is a pleasure for us to thank D. Ouw and J. Jethwa for technical assistance.

[1] A. G. Michette, I. C. E. Turcu, M. S. Schulz, M. T. Browne, G. R. Morrison, P. Fluck, C. J. Buckley, and G. F. Forster, Rev. Sci. Instrum. **64**, 1478 (1993).
[2] A. G. Michette, A. M. Rogoyski, and R. E. Burge, J. Phys. E **21**, 959 (1988).
[3] M. M. Murnane, H. C. Kapteyn, and R. W. Falcone, IEEE J. Quantum Electron. **25**, 2417 (1989).
[4] R. Fedosejevs, R. Ottmann, R. Sigel, G. Kühnle, S. Szatmári, and F. P. Schäfer, Appl. Phys. B **50**, 79 (1990).
[5] M. M. Murnane, H. C. Kapteyn, and R. W. Falcone, Phys. Rev. Lett. **62**, 155 (1989).
[6] D. G. Stearns, O. L. Landen, E. M. Campbell, and J. H. Scofield, Phys. Rev. A **37**, 1684 (1988).
[7] J. C. Kieffer, M. Chaker, C. Y. Côté, Y. Beaudoin, H. Pépin, C. Y. Chien, S. Coe, and G. Mourou, Appl. Opt. **32**, 4247 (1993).
[8] B. M. Penetrante and J. N. Bardsley, Phys. Rev. A **43**, 310 (1991).
[9] S. Szatmári and F. P. Schäfer, Opt. Commun. **68**, 196 (1988).
[10] S. Szatmári, G. Almási, and P. Simon, Appl. Phys. B **53**, 82 (1991).
[11] M. M. Murnane, H. C. Kapteyn, and R. W. Falcone, Appl. Phys. Lett. **56**, 1948 (1990).
[12] B. L. Henke, J. Liesegang, and S. D. Smith, Phys. Rev. B **19**, 3004 (1979).
[13] C. Wülker, W. Theobald, J. S. Bakos, B. van Wonterghem, and F. P. Schäfer, Rev. Sci. Instrum. (to be published).
[14] W. Theobald, C. Wülker, J. Jasny, S. Szatmári, F. P. Schäfer, and J. S. Bakos, Phys. Rev. E **49**, R4799 (1994).
[15] P. Mora, Phys. Fluids **25**, 1051 (1982).
[16] W. L. Kruer, *The Physics of Laser Plasma Interactions* (Addison-Wesley, Reading, MA, 1988).
[17] M. Born and E. Wolf, *Principles of Optics,* 6th ed. (Pergamon, Oxford, 1980).
[18] B. N. Chichkov, Inst. Phys. Conf. Ser. **125**, 223 (1992).
[19] W. L. Wiese, M. W. Smith, and B. M. Glennon, *Atomic Transition Probabilities,* Natl. Bur. Stand. Ref. Data Ser., Natl. Bur. Stand. (U.S.) Circ. No. 4 (U.S. GPO, Washington, DC, 1966).
[20] I. I. Sobel'man, L. A. Vainshtein, and E. A. Yukov, *Excitation of Atoms and Broadening of Spectral Lines,* edited by V. I. Goldanskii *et al.*, Springer Series in Chemical Physics Vol. 7 (Springer, Berlin, 1981).
[21] B. N. Chichkov and E. E. Fill, Phys. Rev. A **42**, 599 (1990).

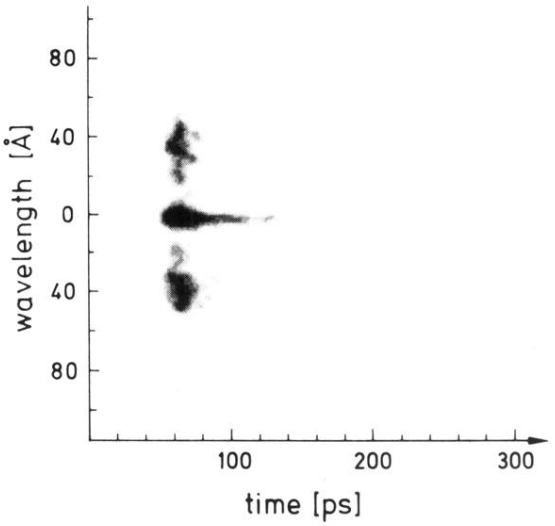

FIG. 2. Density plot from the output of the time-resolving spectrograph. The horizontal axis represents the time, the vertical one the wavelength symmetrically to the zeroth order in the middle of the picture. The picture is a sum of five shots with the SP alone.